CFD Simulation of Kerosene-Fueled Supersonic Combustion Ramjet Combustor Experiments

Wan Tian*, Chen Lihong, Wang Jing, Fan Xuejun, Chang Xinyu

Key Laboratory of High Temperature Gas Dynamics (LHD), Institute of Mechanics, Chinese Academy of Sciences, Beijing, 100190, China

Abstract

The kerosene-fueled scramjet combustor experiments are numerically simulated, for the purpose of code validation and better understanding of flow structure. Full chemically reacting Navier-Stokes equation is numerically solved, and a global reaction mechanism and a reduced 12 species 12 step reaction mechanism are used for kerosene combustion. Computational results using different level of grid refinement and wall boundary conditions are compared with the experimentally measured data. In addition, computed results with different reaction mechanisms are compared. The computed and experimental results agree well. Three dimensional flow structures of different fuel injection scheme are compared. The results show that the subsonic region of the in-cavity fuel injection is located near the sidewall, whereas for the case with upstream single-hole fuel injection, the subsonic region is located near the symmetry plane.

Keywords kerosene fuel; scramjet; combustor; CFD; parallel computation

1. Introduction

Whereas much computational work has been done for hydrogen-fueled Supersonic Combustion Ramjet (scramjet) combustors, supercritical kerosene-fueled scramjet has not beenequally studied by numerical methods. Recently, chemical and physical properties of kerosene combustion have been studied[1-4]. In the present paper, scramjet combustor experiments are numerically simulated, in order to understand the complex physics inside the combustor, as well as validate the computational models. The experiments conducted at Institute of Mechanics, Chinese Academy of Sciences are selected as the benchmark cases. Chemically reacting Navier-Stokes equation is solved, and the turbulence is modeled by a two-equation k-omega SST model. Two reaction mechanisms are used for kerosene combustion: a one-step global mechanism and a 12 species 13 step reduced mechanism. The computed wall pressure distribution matches well with the measured data. The influence of computational mesh is also studied where the maximum mesh size is above two million, and parallel computation with up to 256 CPUs is performed. The influence of reaction mechanism and cold/adiabatic wall boundary conditions is also studied. Two combustor configurations are simulated, one with fuel injection inside the cavity, and the other with fuel injection upstream of the cavity. Both cases with cold main flow without combustion and hot main flow with combustion are simulated, and the computed results agree with the experimental data.

The physical phenomena inside the combustor are examined. Mach number contours show that large separation zone exists inside the combustor and the flow inside the separation zone is subsonic, whereas the core flow near the centerline remains supersonic. There is shock-train inside the isolator, which slows down the flow and increases the pressure at the combustor entrance and hence increases the combustion efficiency. In order for the shock-train to establish, enough heat release has to be added to choke the flow. Results show that the combustion efficiency in a dual-cavity combustor is higher than that of a single-cavity combustor. This is because that the shear layer across the cavity essentially compresses the main flow and makes the main flow easier to be choked. Results also show that there is expansion of the core flow upstream of the cavity. The pressure drop caused by the expansion balances the combustion pressure rise, which explains the nearly constant pressure across the cavity.

2. Computation Scheme

2.1 Governing equation

The full unsteady Navier-Stokes equation is numerically solved. The species conservation equation is given by

$$\frac{\partial \rho_s}{\partial t} + \nabla \cdot (\rho_s \boldsymbol{u}) + \nabla \cdot (\rho_s \boldsymbol{v}_s) = \omega_s \qquad (1)$$

where ρ is density, $\boldsymbol{u}$ is the convection velocity vector, and $\boldsymbol{v}$ is the diffusion velocity vector. t means time, and ω is the source term for chemical reactions. The momentum equations are given by

* Corresponding author. E-mail address: wtsmile@126.com

$$\frac{\partial(\rho \boldsymbol{u})}{\partial t}+\nabla\cdot(\rho \boldsymbol{u}\otimes \boldsymbol{u})+\nabla p+\nabla\cdot\tau=0 \qquad (2)$$

where p is pressure, and τ is the viscous stress tensor. The total energy conservation equation is as follows

$$\frac{\partial E}{\partial t}+\nabla\cdot((E+p)\boldsymbol{u})=-\nabla\cdot\boldsymbol{q}-\nabla\cdot(\boldsymbol{u}\cdot\tau)$$
$$-\nabla\cdot\sum_{s=1}^{ns}(v_s\rho_s h_s) \qquad (3)$$

where E is total energy per unit volume, $\boldsymbol{q}$ is heat flux vector, and h is enthalpy per unit mass. Menter's $k\omega$ SST is used as our turbulence model, together with a compressibility correction for high Mach number flow.

The convection terms of the governing equations are discretized with a third-order upwind MUSCL-TVD method, and the diffusion terms are discretized with a second-order central scheme. The unsteady term is discretized with a second-order scheme, and dual time-step is used.

2.2 Reaction Mechanism

Two reaction mechanisms are used for kerosene combustion: one is a global mechanism; the other is a 12 species 12 step reduced mechanism. The global mechanism[5] is the following

$$C_{12}H_{23}+18O_2\rightarrow 12CO_2+12H_2O$$

where kerosene fuel is approximated by $C_{12}H_{23}$. The reaction rate coefficient is expressed in an Arrehnius form:

$$k_f=AT^n e^{-Ea/T} \qquad (4)$$

For the above global reaction, A of 2.587E+11, n of 0, and Ea of 15105 are used, where the units are cm-K-s-mole. The reduced mechanism[6] is listed in Tab. 1.

Tab. 1 Reduced mechanism of kerosene combustion

Reaction	A	n	Ea
$2C_{12}H_{23}+12O_2\rightarrow 24CO+23H_2$	1.80E11	0.0	15105
$\{O\}+N_2+O_2\rightarrow 2NO+\{O\}$	2.40E02	0.5	22105
$\{N_2\}+2NO\rightarrow N_2+O_2+\{N_2\}$	5.00E14	0.0	4028
$H_2+O\Leftrightarrow H+OH$	2.50E16	0.0	3021
$H_2+OH\Leftrightarrow H_2O+H$	1.00E11	1.1	1823
$H+O_2\Leftrightarrow O+OH$	4.00E14	0.0	9063
$2O_2\Leftrightarrow 2O+O_2$	7.50E18	0.0	56515
$\{N_2\}+2H\Leftrightarrow H_2+\{N_2\}$	2.00E17	0.0	0
$CO+OH\Leftrightarrow CO_2+H$	1.51E07	1.3	382
$N_2+O\Leftrightarrow N+NO$	6.50E13	0.0	37769
$N+O_2\Leftrightarrow NO+O$	6.30E09	1.0	3162
$N+OH\Leftrightarrow NO+H$	3.00E11	0.0	0

2.3 Experiments setup

The experiments consist of two sets: one with cold inflow and the other set with hot inflow. The schematic drawing of the model combustor is shown in Fig. 1. The model combustor has two configurations: one has two sets of dual-cavity, and the other has one set of cavities. Configuration Ⅰ:

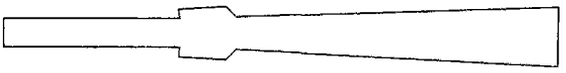

Configuration Ⅱ:

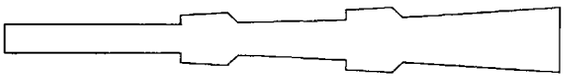

Fig. 1 Schematic drawing of the model combustor.

Configuration I is used for the experiment with cold incoming flow. The cold flow has total temperature of 1470K, total pressure 1.32MPa, and mass flow rate of 1790g/s. The Mach number is 2.35. The vitiated incoming air contains 60.8% nitrogen and 20.8% oxygen, and the rest is H_2O. Supercritical kerosene is injected from a single hole of 4mm diameter, which is located 60mm upstream of the cavity. The mass flow rate of the kerosene fuel is 122g/s, and its total temperature and pressure is 750K and 5.1MPa, respectively.

For experiments with hot flow, both configuration I and II are used. For configuration I, the incoming flow has total temperature of 1800K, total pressure of 1.30MPa, mass flow rate of 1540g/s, Mach number of 2.35. Supercritical kerosene fuel is injected from a single hole of 4mm diameter, which is located 60mm upstream of the cavity. The combustion equivalence ratio is 0.7. For configuration II, the incoming flow has total temperature and pressure of 1800K and 1.11MPa, respectively. The mass flow rate is 1340g/s, and the Mach number is 2.33. The composition of the vitiated air is 56.8% nitrogen, 19.2% oxygen and the rest is water. Supercritical kerosene fuel is injected from five holes of 1.2mm diameter, which are located at the floor in the upstream cavities. The combustion equivalence ratio is 0.72. For both configurations, pilot hydrogen is injected from 5 holes located 5mm upstream of the upstream cavities. The equivalence ratio of the pilot hydrogen is about 0.09.

Two computational grids are used, which have different level of refinement. The coarse grid has 0.9 million points, and the refined grid has 2.1 million grids. The refinement is made near the injection holes, as well as in the stream-wise and vertical direction. Both constant temperature and adiabatic wall boundary condition are used. The computation was conducted by using parallel computers up to 256 CPUs.

3. Presentation of Result

Fig. 2 plots the pressure distribution along the

centerline of the sidewall for the cold inflow case. The symbols are experimentally measured data, and the line is the computed result. It shows that the experimental and computed results agree well. The computation captures the important flow features including the injection induced bow shock and the shock reflections.

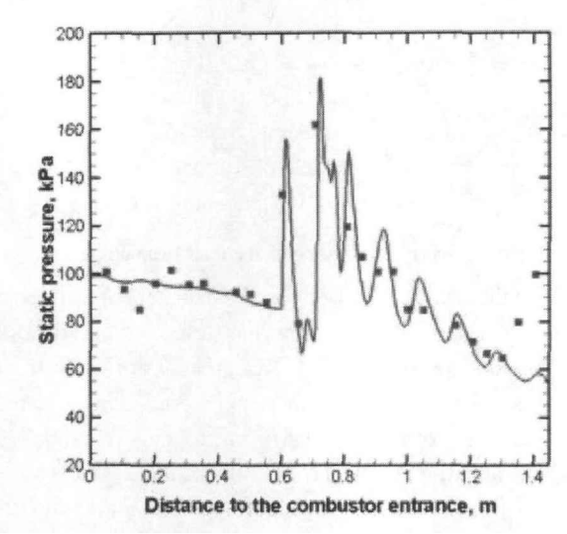

Fig. 2 Comparison between computation and experiment results for the cold inflow case. Plotted is the static pressure along the sidewall centerline. The symbols are the measured data, and the line is the computed result

Fig. 3 plots the pressure distribution along the centerline of the sidewall for the hot inflow case, where the kerosene fuel is injected from the floor of the upstream cavities. The figure shows that the computed results agree with the measured pressure in general. The difference between the coarse grid and the refined grid exists in the upstream end of the shock train. The refined grid result shows shocks near the sidewall, whereas the coarse grid does not, which might be caused by numerical diffusion. Except for that, both grids produce similar results.

Fig. 4 plots the pressure distribution along the sidewall centerline for the hot inflow case, where the kerosene fuel is injected upstream of the cavities. Results using different wall boundary conditions and reaction mechanisms are compared. The results show that adiabatic wall condition leads to larger maximum pressure and longer shock train than constant temperature wall condition. The result with reduced mechanism agrees well with the measured pressure, whereas the results with global mechanism over-predict the length of the shock train. These results are expected, as adiabatic wall and global mechanism lead to larger heat addition to the flow, which results in larger maximum pressure and longer shock train.

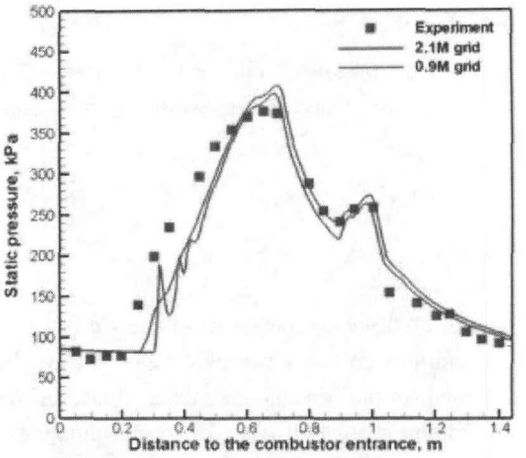

Fig. 3 Comparison between computation and experiment results for the hot inflow case, where fuel is injected from the upstream cavity floor. Plotted is the static pressure along the sidewall centerline. The symbols are the measured data, and the line is the computed result

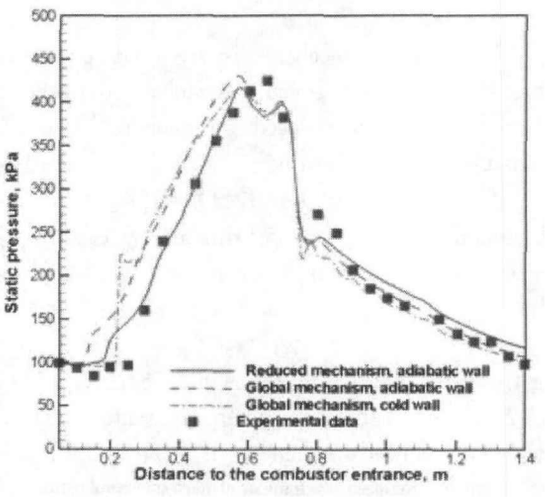

Fig. 4 Comparison between computation and experiment results for the hot inflow case, where fuel is injected upstream of the cavity. Plotted is the static pressure along the sidewall centerline. The symbols are the measured data, and the line is the computed result

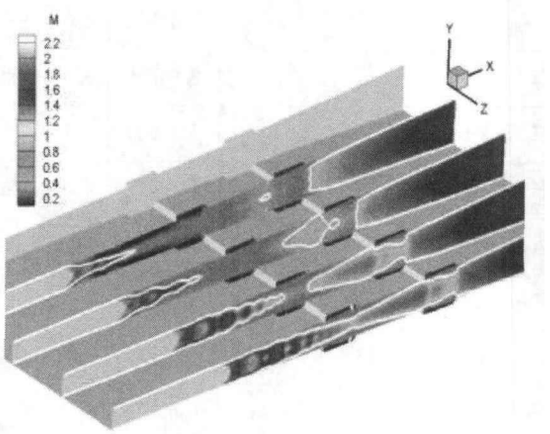

Fig. 5 Mach contour slices of the hot inflow case, where the fuel is injected from the floor of the upstream cavities. The dimension in the span-wise direction is increased 20 times for clarity

Fig. 5 and 6 plot the Mach contour slices along the stream-wise direction. The case with fuel injected from the cavity floor is shown in Fig. 5, and the case with fuel injected upstream of the cavity is shown in Fig. 6. The white lines in both figure are the sonic line. The figures show the existence and structure of the pre-combustion shock train. In both cases, a large portion of the cavity region is subsonic. The supersonic region in Fig. 5 is located near the symmetric plane, whereas in Fig. 6 it is located near the sidewall. This is because in Fig. 6, the fuel is injected from a single hole located at the symmetry plane, and hence the combustion region exists near the symmetry plane. In the combustion region the temperature is high, which leads to subsonic flow.

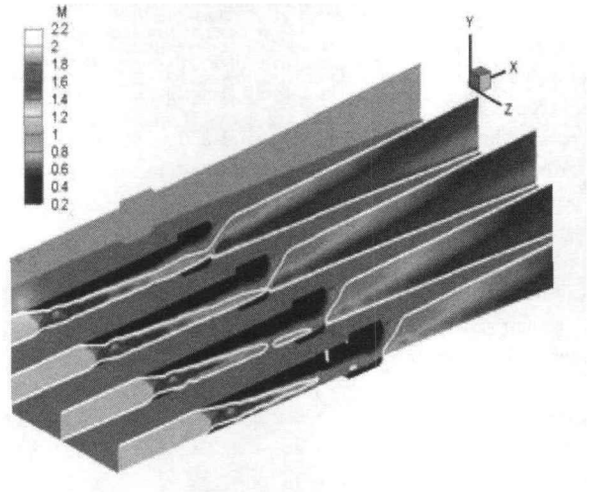

Fig. 6 Mach contour slices of the hot inflow case, where the fuel is injected upstream of the cavities. The dimension in the span-wise direction is increased 20 times for clarity

4. Conclusions

(1)The kerosene-fueled scramjet combustor experiments are numerically simulated. The simulated experiments include cold and hot incoming flow, as well as different fuel injection schemes. The results show that our computation method and code can simulate the pressure distribution after comparison with the experimental data.

(2)Computations with different wall boundary condition and grid refinement are compared. Three dimensional flow structures of different fuel injection scheme are compared. The results show that the subsonic region of the in-cavity fuel injection is located near the sidewall, whereas for the case with upstream single-hole fuel injection, the subsonic region is located near the symmetry plane.

References

[1] Fan X, Yu G, Li J, Lu X, Zhang X, Combustion and Ignition of Thermally Cracked Kerosene in Supersonic Model Combustors. Journal of Propulsion and Power, Vol. 23, No. 2, 2007.

[2] Wang T, Thermophysics Characterization of Kerosene Combustion, Journal of Thermophysics and Heat Transfer, Vol. 15, No. 2, 2001.

[3] Edwards T, Maurice L, Surrogate Mixtures to Represent Complex Aviation and Rocket Fuels. Journal of Propulsion and Power, Vol. 17, No. 2, 2001.

[4] Yang S, Le J, Zhao H, Zhen Z, Three-Dimensional Massively Parallel Simulation of Kerosene-Fueled Scramjet Engine [In Chinese]. Computational Physics. No. 4, 2009.

[5] Lee C, Kundu K, Ghorashi B, Simplified Jet-A Kinetic Mechanism for Combustor Application. AIAA Paper 930021.

[6] Kundu K, Penko P, Reduced Reaction Mechanisms for Numerical Calculation in Combustion of Hydrocarbon Fuels. AIAA Paper 980803.